

RE-SORT: Removing Spurious Correlation in Multilevel Interaction for CTR Prediction

Abstract

Click-through rate (CTR) prediction is a critical task in recommendation systems, serving as the ultimate filtering step to sort items for a user. Most recent cutting-edge methods primarily focus on investigating complex implicit and explicit feature interactions; however, these methods neglect the spurious correlation issue caused by confounding factors, thereby diminishing the model’s generalization ability. We propose a CTR prediction framework that **RE**moves **Spurious cOR**relations in **mulT**ilevel feature interactions, termed **RE-SORT**, which has two key components. I. A multilevel stacked recurrent (MSR) structure enables the model to efficiently capture diverse nonlinear interactions from feature spaces at different levels. II. A spurious correlation elimination (SCE) module further leverages Laplacian kernel mapping and sample reweighting methods to eliminate the spurious correlations concealed within the multilevel features, allowing the model to focus on the true causal features. Extensive experiments conducted on four challenging CTR datasets, our production dataset, and an online A/B test demonstrate that the proposed method achieves state-of-the-art performance in both accuracy and speed. The utilized codes, models and dataset will be released at <https://github.com/RE-SORT>.

1 INTRODUCTION

Click-through rate (CTR) prediction holds significant importance in recommendation systems [Fan et al., 2023, Ye et al., 2022, Rendle et al., 2009] and online advertising scenarios. The objective of this task is to gauge the likelihood of a user clicking on a recommended item or an advertisement displayed on a web page. Developing more effective methods

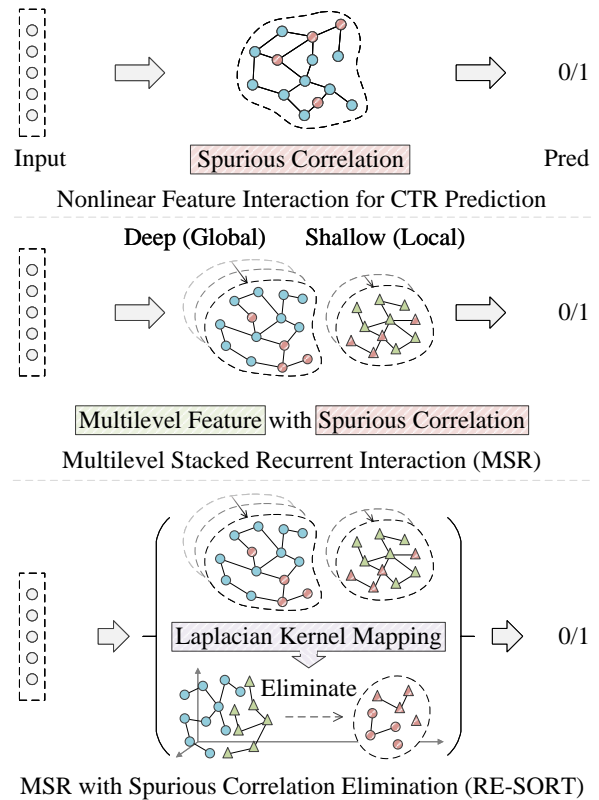


Figure 1: RE-SORT exploits multilevel features with spurious correlation elimination for CTR prediction.

for modeling user and item features has emerged as a crucial research challenge in the CTR prediction field.

To learn comprehensive feature interactions, various models have been developed. On the one hand, Xiao et al. [2017], Rendle [2010], Pan et al. [2018], and Sun et al. [2021] learn low-order feature interactions to achieve low temporal and spatial complexity. However, relying solely on first-order and second-order feature interactions results in limited performance [Juan et al., 2016]. On the other hand, models such as AutoInt [Song et al., 2019] and SAM [Cheng and Xue,

2021] employ self-attention mechanisms to capture high-order feature interactions, thereby enhancing their representation capabilities. To further incorporate richer high-order features, two-stream CTR models that leverage dual parallel networks to capture feature interactions from distinct perspectives (e.g., explicit vs. implicit perspectives) have been developed. For instance, the DCN [Wang et al., 2017] automates the feature cross-coding process through linear and nonlinear feature learning streams. Building upon the DCN, the GDCN [Wang et al., 2023] introduces a soft gate to the linear feature learning stream to filter important features. In contrast with the DCN and GDCN, FinalMLP [Mao et al., 2023] uses two nonlinear feature learning streams to implicitly encode the features at distinct levels by setting multilayer perceptrons (MLPs) with different parameters.

While the existing two-stream methods have achieved superior performance by diversifying the features through the introduction of various feature interaction streams, there is still substantial room for improvement in implicitly constructing hierarchical features within each stream (please refer to Section 4.3 for the experimental validation). Previous works such as [Du et al., 2021] and [Pascanu et al., 2013] have demonstrated that stacked recurrent structures can learn more intricate representations compared to the feed-forward structures such as MLP structures, allowing each layer to potentially represent different levels of abstraction. By restoring the previous state in the recurrent structure [Quadrana et al., 2017], the use of a greater number of stacks leads to better integrated global high-level representations (e.g., the coarse-grained common patterns of the user preferences for recommended items), while the use of fewer stacks results in increased feature combinations with local details (e.g., the fine-grained associations between users and items). To more effectively differentiate among the hierarchical distinctions of the features in each stream, we propose a two-stream multilevel stacked recurrent (MSR) structure that leverages the capacity of the network to capture both global and local features. Based on the proposed stacked recurrent structure, an acceleration module is further introduced to substantially boost the inference efficiency of the proposed approach.

Furthermore, although the two-stream structure can extract richer multilevel features, as illustrated in Figure 1 (rows 1 and 2), it is still hindered by the presence of “spurious correlations”, which refer to statistical relationships between two or more variables that appear to be causal but are not causal. These spurious correlations inherently arise from the subtle connections between noisy features and causal features [Li et al., 2022], which reduces the model’s generalization ability [Lu et al., 2021]. For example, in movie recommendation tasks, the prominence of certain trending films may result in higher click counts due to their prioritized placements. However, the actual preferences of users might not align with the genres or contents of these trend-

ing movies. This creates spurious correlations between the popularity of certain film types and the genres that users truly appreciate, and movie placement is the confounding factor. Recent studies [Mao et al., 2023, Wang et al., 2021a, Guo et al., 2017] have confirmed through meticulous parameter analyses that model performance decreases when the interaction order exceeds a certain depth, typically three orders [Wang et al., 2023], and one of the crucial reasons for this is the exacerbation of the spurious correlation issue. Previous works [Wang et al., 2021a, 2023] have used gating mechanisms to assign varying levels of importance to different features. However, in the absence of a supporting causal theory [Guan et al., 2023], feature selection methods fail to identify the true causal features, instead favoring features that arise from spurious correlations. LightDIL [Zhang et al., 2023] divided historical data into multiple periods chronologically, forming a set of environments, and learned stable and practical feature interactions within these environments, yet its effectiveness diminishes when users have constrained click histories.

As shown in Figure 1 (row 3), to address the spurious correlation issue, we employ the Laplacian kernel function to project low-dimensional feature interactions into a high-dimensional space. Thus, nonlinear transformations can be achieved in the low-dimensional space through a linear transformation in the high-dimensional space. Then, we use a sample reweighting strategy that learns different weights for various instances during training to eliminate spurious correlations. The detailed theory is explained in Section 3.5. Leveraging the combined power of the MSR and SCE, we have exploited the network’s ability to eliminate the spurious correlations concealed within the hierarchical feature spaces, which enhances the CTR prediction process. The contributions are summarized as follows:

- We propose a CTR prediction framework that removes spurious correlations in multilevel feature interactions; this approach leverages the hierarchical causal relationships between items and users to fundamentally enhance the model’s generalization ability.
- We propose a multilevel stacked recurrent (MSR) structure, which efficiently builds diverse feature spaces to obtain a wide range of multilevel high-order feature representations.
- We introduce a spurious correlation elimination (SCE) module, which utilizes Laplacian kernel mapping and sample reweighting methods to eliminate the spurious correlations hidden in multilevel feature spaces.
- The results of extensive experiments conducted on four challenging CTR datasets, our production dataset, and an online A/B test demonstrate that the proposed RE-SORT achieves state-of-the-art (SOTA) performance in terms of both accuracy and speed.

2 RELATED WORKS

2.1 RECURRENT STRUCTURE

Recurrent structures have found widespread application in various research fields, including computer vision (CV) and natural language processing (NLP). For instance, in stereo matching, a recurrent hourglass network is proposed by Du et al. [2021] to effectively capture multilevel information. This strategy enhances the adaptability of the network to complex scenarios by leveraging comprehensive global and local features. In the realm of recommendation systems, DRIN [Jun et al., 2022] employs a recurrent neural network (RNN) with 1×1 convolution kernels to recurrently model the second-order feature interactions between a raw feature and the current feature. However, DRIN utilizes only a single vanilla RNN branch, overlooking the potential benefits of a two-stream structure with varying stacking depths for simultaneously capturing both global and local feature representations. In contrast, our two-stream MSR structure is equipped with a self-attention mechanism, attenuation units, and an acceleration method. This design fundamentally enhances the capacity of the network to efficiently capture multilevel high-order features.

2.2 SPURIOUS CORRELATION IN RECOMMENDATION TASKS

In the field of causal inference, causality refers to the cause-effect relationship between variables, where changes in one variable trigger changes in another variable. The objective is to identify these relationships. Conversely, a spurious correlation refers to an observed association that does not necessarily indicate a genuine causal connection, which often occurs due to the presence of confounding variables or selection bias [Spirtes et al., 2013]. Dou et al. [2022] utilized feature decorrelation to promote feature independence, thereby mitigating spurious textual correlations for natural language understanding. Zhang et al. [2021] employed sample reweighting for variable decorrelation tasks to identify stable features for image classification. In recommendation tasks, Li et al. [2022] incorporated causal feature selection into factorization machines (FMs) to address the issue of confounding factors and selection bias, thereby improving the robustness of the output recommendations. They learned the weights associated with each first-order and second-order feature to explicitly select causal features. However, not all causal features are limited to these orders, and the employed optimization method hinders efficiency, particularly when handling many features. In contrast, our proposed method not only learns the weight of every instance to select causal features and feature interactions with arbitrary orders but also boasts an efficient structure with a rapid inference speed, providing a more comprehensive approach.

3 METHOD

In this section, we introduce the proposed MSR and SCE, the CTR predictor, the loss function, and the theory behind the sample reweighting method in the SCE module.

3.1 MULTILEVEL STACKED RECURRENT (MSR) INTERACTION

The adoption of a two-stream model structure for CTR prediction stems from insights gleaned from prior research and practical applications [Wang et al., 2023, Mao et al., 2023, Wang et al., 2021b,a]; this structure helps enhance the expressiveness of the constructed model. Following previous works, the proposed MSR method contains two streams: a deeply stacked recurrent (D-SR) stream and a shallow stacked recurrent (S-SR) stream. As shown in Figure 2, each stream includes multiple stacked recurrent blocks with a self-attention structure and varying attenuation coefficients, thus enhancing the depth-based pattern and dependency learning process. The input feature of both D-SR and S-SR is denoted as x_0 , and the outputs of D-SR and S-SR are denoted as F_d and F_s , respectively. The calculation process is defined as: $F_d = \text{D-SR}(x_0)$, $F_s = \text{S-SR}(x_0)$. We take the i -th block of the D-SR as an example. Given an input x_{i-1} , we first project it into a one-dimensional function w_v : $V_i = x_{i-1} \cdot w_v$ and then map V_i to x_i through the state S_i . We recurrently calculate the output as follows:

$$S_i = r_i S_{i-1} + K_i^T V_i, \quad (1)$$

$$x_i = \text{SR}_i(x_{i-1}) = Q_i S_i, \quad (2)$$

where SR_i denotes the i -th block, Q_i , K_i , and V_i are projections, r_i is the attenuation coefficient, and $i \in 1, 2, 3, \dots, M$. We further add a swish gate [Ramachandran et al., 2017] in each stream to increase the non-linearity of MSR layers.

Enhancing computational efficiency in MSR. In addition, we find that many weights in the softmax function are applied to abnormal or null values, which results in unnecessary computational costs. Therefore, we propose changing the softmax function to learnable matrices by using a relative position encoding [Sun et al., 2022] in the stacked recurrent structure to reduce the incurred temporal and spatial costs.

Formally, we construct the layer as shown in Algorithm 1, where P_Z and P_U are learnable matrices used to replace the softmax function, and ‘‘GroupNorm’’ [Shoeybi et al., 2019] normalizes the output of each block. In summary, the different depths of the D-SR and S-SR streams lead to significant differences among the learning feature interactions of any order, enabling the model to grasp the global and local dependencies at various abstraction levels.

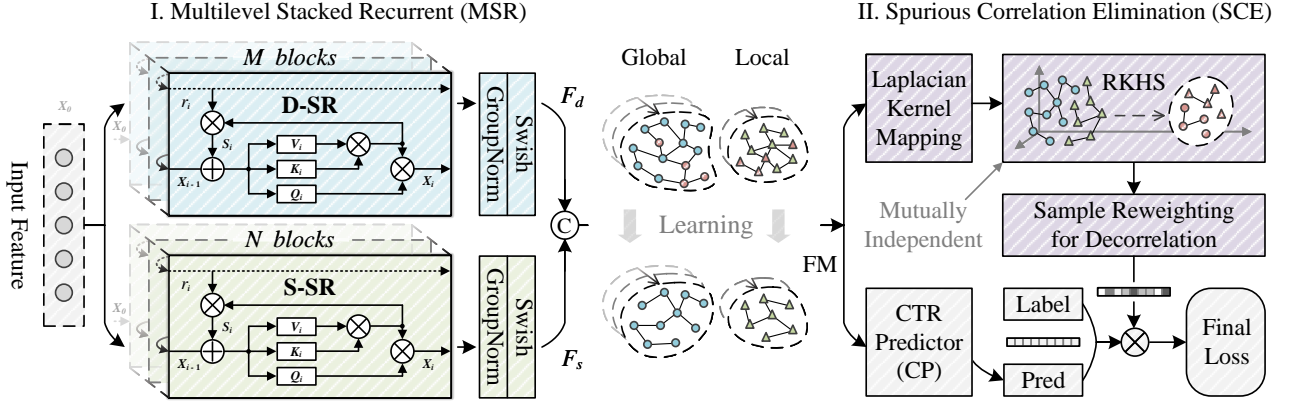


Figure 2: Overview of the RE-SORT framework, which contains two key components: I. a multilevel stacked recurrent (MSR) structure and II. a spurious correlation elimination (SCE) module. The deep and shallow stacked recurrent interactions (D-SR and S-SR) in the MSR structure and the SCE module are colored blue, green, and purple, respectively. The D-SR and S-SR streams contain M and N ($M > N$) stacked blocks, and “ Q_i ”, “ K_i ”, and “ V_i ” denote the query, key, and value, respectively, for i -th block. The attenuation coefficient is denoted by r_i for i -th block (dotted lines). The outputs F_d and F_s are concatenated (“C”) as the input of the SCE and the CTR predictor, which is visualized to show the spurious correlation elimination process guided by the SCE module. “RKHS” denotes the reproducing kernel Hilbert space. The SCE procedure is explained in Algorithm 2.

Algorithm 1 The procedure of D-SR

Input: Input data x_0 , Attenuation coefficient r_i , Learnable matrices P_Z , P_U , Blocks number: M

Output: F_d

- 1: $x_1 \leftarrow \text{SR}_1(x_0, r_1)$
 - 2: **for** $i \leftarrow 2$ **to** M **do**
 - 3: $x_i \leftarrow \text{SR}_i(x_{i-1}, r_i)$
 - 4: **end for**
 - 5: $T \leftarrow \text{GroupNorm}([x_1, x_2, \dots, x_M])$
 - 6: $F_d \leftarrow (\text{swish}(x_0 \cdot P_Z) \odot T) \cdot P_U$
 - 7: **return** F_d
-

3.2 SPURIOUS CORRELATION ELIMINATION

Since we’ve established distinct feature spaces with the MSR, our next objective is to eliminate the spurious correlations concealed within them. We concatenate the last two outputs F_d, F_s to form a local feature map FM.

Statistical independence assessment. To eliminate spurious correlations, we use sample reweighting to make the spurious correlations independent of the user click behavior prediction task y_i . The underlying theory is elaborated upon in Section 3.5 and the supplementary materials. Specifically, inspired by the kernel function in a support vector machine (SVM), we map the features into a high-dimensional space with a Laplacian kernel. In the high-dimensional space, we eliminate the spurious correlations between features with nonlinear operations corresponding to the original feature space. We use X and Y to denote the features, and the SCE module measures the dependence between them. The theory

regarding why SCE measures dependence is also given in the supplementary materials.

$$\text{SCE}(X, Y) = \|K_X - K_Y\|_{\text{FN}}, \quad (3)$$

where $K_X = k_X(X, X)$ and $K_Y = k_Y(Y, Y)$ are Laplacian kernel matrices, $\|\cdot\|_{\text{FN}}$ is the Frobenius norm (FN) which corresponds to the Hilbert-Schmidt norm in Euclidean space [Strobl et al., 2019], and k_X and k_Y are Laplacian kernels that can capture local patterns and are robust to outliers. However, applying the SCE approach with large-scale kernel matrices can be computationally expensive. Therefore, we use random Fourier features (RFFs) to approximate the Laplacian kernel. Afterwards, the reconstructed features can be obtained in the new representation space, which reduces the temporal complexity of the network from $O(n^2)$ to $O(n)$.

$$\mathcal{H}_{\text{RFF}} = \{h : x \rightarrow \sqrt{2} \cos(wx + \phi) \mid w \sim N(0, 1), \phi \sim U(0, 2\pi)\}, \quad (4)$$

where \mathcal{H}_{RFF} denotes the function space of RFF, \square is sampled from the standard normal distribution, and ϕ is sampled from the uniform distribution.

We define the partial cross-covariance matrix as the measure of covariance between the two sets of features:

$$\text{SCE}_{\text{RFF}}(X, Y) = \|C_{p(X), q(Y)}\|_{\text{FN}}^2 \quad (5)$$

$$= \sum_{i=1}^{n_X} \sum_{j=1}^{n_Y} |\text{Cov}(p_i(X), q_j(Y))|^2, \quad (6)$$

where X and Y represent features, p and q are random Fourier feature mapping functions, n_X and n_Y are the number of functions from \mathcal{H}_{RFF} , $\|\cdot\|_{\text{FN}}$ is the Frobenius norm

Algorithm 2 Procedure of SCE module

Input: Balancing epoch number, Batch size**Output:** Trained model with weight w_{result}

- 1: Define: n : the number of random Fourier space
 - 2: Initialize: sample weights: $w_{\text{result}} = [1, 1, \dots, 1]$
 - 3: Reload global features and weights as Eq. (12), Eq. (13)

 - 4: **for** batch $\leftarrow 1$ **to** Batch size **do**
 - 5: **for** epoch balancing \leftarrow Balancing epoch number **to** 1 **do**
 - 6: $n_X = n_Y =$ epoch balancing
 - 7: Optimize w_{result} with n_X and n_Y as Eq. (11)
 - 8: **end for**
 - 9: Back propagate with weighted prediction loss as Eq. (18)
 - 10: Save features and weights in GFI' and GWI' as Eq. (14), Eq. (15)
 - 11: **end for**
-

(FN), and $C_{p(X),q(Y)} \in \mathbb{R}^{n_X \times n_Y}$ is the cross-covariance matrix of random Fourier features $p(X)$ and $q(Y)$ containing entries:

$$p(X) = (p_1(X), \dots, p_n(X)), p_i(X) \in \mathcal{H}_{\text{RFF}}, \forall i, \quad (7)$$

$$q(Y) = (q_1(Y), \dots, q_n(Y)), q_j(Y) \in \mathcal{H}_{\text{RFF}}, \forall j. \quad (8)$$

Global sample weight optimization. In this section, we present a method for optimizing the global features and global sample weights to enhance the performance of the model. Our approach aims to effectively capture features and assign appropriate weights to the samples. By iteratively updating the feature weights and incorporating global and local information, we can improve the feature representations and their integration into the model. By minimizing $\text{SCE}_{\text{RFF}}^w(X, Y)$, we encourage feature independence, resulting in a more causal and consistent covariate matrix. For any two features $X_{:,a}, X_{:,b} \in X$, the weighted spurious correlation elimination process is $\text{SCE}_{\text{RFF}}^w(X, Y)$.

$$\begin{aligned} \text{SCE}_{\text{RFF}}^w(X_{:,a}, X_{:,b}, w) \\ = \sum_{i=1}^{n_X} \sum_{j=1}^{n_Y} |\text{Cov}(p_i(w^T X_{:,a}), q_j(w^T X_{:,b}))|^2. \end{aligned} \quad (9)$$

In each iteration, our objective is to minimize the sum of Eq. (9). Therefore, the resulting weight is

$$\begin{aligned} w_{\text{result}} &= \arg \min_w \sum_{1 \leq a \leq b \leq m} \text{SCE}_{\text{RFF}}^w(X_{:,a}, X_{:,b}, w) \quad (10) \\ &= \arg \min_w \sum_{1 \leq a \leq b \leq m} \sum_{i=1}^{n_X} \sum_{j=1}^{n_Y} |\text{Cov}(u_i, v_j)|^2, \end{aligned} \quad (11)$$

where $u_i = p_i(w^T X_{:,a})$, $v_j = q_j(w^T X_{:,b})$. To avoid local optima, we incorporate global information. We employ a memory module consisting of GFI and GWI. GFI captures global feature information, while GWI stores global weight information. The features and weights are used to optimize the new sample weights.

$$\text{GFI}_i = \text{Concat}(\text{GFI}_{i-1}, \text{FM}_i), \quad (12)$$

$$\text{GWI}_i = \text{Concat}(\text{GWI}_{i-1}, w_i), \quad (13)$$

where $\text{GFI}_1 = \text{FM}_1$, $\text{GWI}_1 = w_1$, FM_i denotes the local feature information, w_i is the local weight information, and i is means the number of iterations. We globally update the features and weights as follows:

$$\text{GFI}'_i = \frac{1}{2}(\text{GFI}'_{i-1} + \text{FM}_i), \quad (14)$$

$$\text{GWI}'_i = \frac{1}{2}(\text{GWI}'_{i-1} + w_i), \quad (15)$$

where $\text{GFI}'_1 = \frac{1}{2}\text{FM}_1$ and $\text{GWI}'_1 = \frac{1}{2}w_1$.

3.3 CTR PREDICTOR

We divide the F_d and F_s into k chunks denoted as $F_d = [F_{d_1}, \dots, F_{d_k}]$, $F_s = [F_{s_1}, \dots, F_{s_k}]$, where k is a hyperparameter. F_{d_j} and F_{s_j} denote the j -th chunk feature of the D-SR and S-SR outputs, respectively. We apply the CTR predictor (CP) to each paired chunk group consisting of F_{d_j} and F_{s_j} . The chunk computations are then aggregated using sum pooling to derive the final predicted probability:

$$\text{CP}(F_{d_j}, F_{s_j}) = b + w_{d_j}^T F_{d_j} + w_{s_j}^T F_{s_j} + F_{d_j}^T W_j F_{s_j}, \quad (16)$$

$$\hat{y} = \sigma\left(\sum_{j=1}^k \text{CP}(F_{d_j}, F_{s_j})\right), \quad (17)$$

where w_{d_j} , w_{s_j} , and W_j are learnable weights, and σ is the sigmoid activation function. Modeling the second-order interactions between hierarchical features $F_{d_j}^T W_j F_{s_j}$ actually involves modeling arbitrary-order feature interactions.

3.4 LOSS FUNCTION

We introduce a reweighting scheme for each sample within the commonly utilized binary cross-entropy loss. This involves applying a distinct weight to the loss of each sample during training.

$$L = - \sum_{i=1}^N w_{\text{result}_i} (y_i \log(\hat{y}_i) + (1 - y_i) \log(1 - \hat{y}_i)), \quad (18)$$

where N is the number of examples, y_i is the true label of instance i , and \hat{y}_i is the predicted probability of a click. During training, we use the weight $w_{\text{result}} = [w_{\text{result}_1}, w_{\text{result}_2}, \dots, w_{\text{result}_N}]$ of the N LogLoss values calculated for every input sample with the sample reweighting mechanism to conduct gradient descent.

Datasets	# Samples	# Fields	# Features
Criteo	45,840,617	39	2,086,936
Avazu	40,428,967	23	1,544,250
Frappe	288,609	10	5,382
MovieLens	2,006,859	3	90,445
UGC	1,015,236,921	92	10,640,310

Table 1: Statistics of the evaluation datasets.

3.5 THE THEORY BEHIND SAMPLE REWEIGHTING

In the following section, we denote the covariate features as $FM=[FM_{rob}, FM_{fal}]$, where FM_{rob} denotes the robust features, and $FM_{fal} = FM/FM_{rob}$ denotes spurious correlation features. $g(\cdot)$ is a nonlinear function learned by the model with FM_{rob} and FM_{fal} . $\beta_{FM_{rob}}$ and $\beta_{FM_{fal}}$ denote the linear weights of FM_{rob} and FM_{fal} . He et al. [2023] demonstrate that $\beta_{FM_{fal}}$ asymptotically exceeds 0, implying that models without the SCE module inevitably suffer from the impact of spurious correlation features. Additionally, the correlation between FM_{rob} and $g(FM_{rob})$ exhibits less variation than the correlation between FM_{fal} and $g(FM_{rob})$ when exposed to parameter variance. Even when sample reweighting is applied randomly, the estimate of $\beta_{FM_{rob}}$ is more robust and less variable than the estimate of $\beta_{FM_{fal}}$. When predicting y_i , y_i and FM_{fal} must be statistically independent of the minimal and optimal predictor FM_{rob} : $y_i \perp FM_{fal} | FM_{rob}$. Xu et al. [2022] prove that FM_{rob} is the minimal and optimal predictor if and only if FM_{rob} is the minimal robust feature set. Therefore, we intend to capture the minimal robust feature set FM_{rob} to obtain robust prediction results. We denote the robust feature set as the minimal robust feature set for simplicity. Let \mathcal{W} be a set of sample weighting functions. Our objective is to acquire \mathcal{W}_{\perp} , a subset of \mathcal{W} in which the features in FM are mutually independent. Zhou et al. [2022] prove that there exists a weight function $w \in \mathcal{W}$ that makes the spurious correlations independent of y_i for linear models. Moreover, Xu et al. [2021b] prove that whether the data generation process is linear or nonlinear, conducting a weighted least squares (WLS) operation using the weighting function in \mathcal{W}_{\perp} can lead to the selection of perfect features. Therefore, we transform the task from finding minimal robust features to obtaining an independent FM by sample reweighting.

4 EXPERIMENTS

4.1 DATASETS AND EVALUATION METRICS

We conduct extensive experiments on four official datasets, our production dataset, and an online A/B test. Table 1 provides an overview of the statistical information. We utilize two evaluation metrics, the area under the ROC curve (AUC)

and LogLoss (cross-entropy loss).

Criteo¹. Criteo is an online advertising and CTR prediction dataset that includes real-world displayed ads.

Avazu². Avazu is a widely used dataset in CTR prediction. This dataset includes real-world advertising data, focusing on mobile ads and user demographics.

Frappe³. Frappe includes smartphone sensor data, which is popular in human activity recognition research.

MovieLens³. MovieLens is used in recommender systems and leverages its movie ratings data to predict the likelihood of a user clicking on a movie.

User Game Content (UGC). The UGC dataset consists of clicking behavior data for user game content collected from our online service over one month. We collected clicking logs with anonymous user IDs, user behavior histories, game content features (e.g., categories), and context features (e.g., operation time).

4.1.1 Baseline

To fairly and accurately verify the improvements achieved by the proposed MSR structure and SCE module, we use a two-stream MLP network as the ‘‘Baseline’’ method. The MLP sizes of the two branches are set to [400, 400, 400] and [800] as these values yield the best performance. This approach aligns with established best practices for two-stream CTR models [Mao et al., 2023], providing a solid foundation for evaluating any modifications or novel approaches in a controlled manner. To further verify the superiority of the proposed recurrent structure, we utilize a self-attention structure to replace the MLP in the ‘‘Baseline’’ model and denote it as ‘‘Baseline + SA’’. The implementations of these models can be found in our open-source code.

4.1.2 Implementation

To conduct fair comparisons with the recently proposed cutting-edge methods, we use the released preprocessed datasets produced by Cheng et al. [2020] with the same splitting and preprocessing procedures. All the models and experiments are implemented based on the FuxiCTR toolkit [Zhu et al., 2021]. RE-SORT and the ‘‘Baseline’’ model follow the same experimental settings as those of FinalMLP [Mao et al., 2023], with the batch size for all datasets set to 4,096, the embedding size set to 10 for the five datasets, and the learning rate set to 0.001 unless otherwise specified. The number of chunks k in the CP is set to 50 for Criteo and UGC, 10 for Avazu and MoiveLens, and 1 for Frappe. The remaining hyperparameters are kept constant for the five

¹<http://labs.criteo.com>

²<https://www.kaggle.com>

³<https://github.com/openbenchmark/BARS>

Class	Model	Criteo		Avazu		MovieLens		Frappe	
		AUC \uparrow	Logloss \downarrow						
First-Order	LR [Richardson et al., 2007]	0.7874	0.4551	0.7574	0.3944	0.9449	0.2870	0.9394	0.2407
Second-Order	FM [Rendle, 2010]	0.8028	0.4514	0.7618	0.3910	0.9551	0.2328	0.9707	0.2003
	AFM [Xiao et al., 2017]	0.8050	0.4434	0.7598	0.3921	0.9568	0.2224	0.9612	0.2182
High-Order	HOFM (3rd) [Blondel et al., 2016]	0.8052	0.4456	0.7690	0.3873	0.9573	0.2075	0.9701	0.2006
	NFM [He and Chua, 2017]	0.8072	0.4444	0.7708	0.3876	0.9682	0.2064	0.9765	0.1694
	OPNN [Qu et al., 2016]	0.8096	0.4426	0.7718	0.3838	0.9566	0.2333	0.9812	0.1912
	CIN [Xu et al., 2021a]	0.8086	0.4437	0.7739	0.3839	0.9666	0.2066	0.9796	0.1676
	AFN [Cheng et al., 2020]	0.8115	0.4406	0.7748	0.3834	0.9656	0.2440	0.9791	0.1853
	AutoInt [Song et al., 2019]	0.8128	0.4392	0.7725	0.3868	0.9633	0.2155	0.9743	0.2315
	SAM [Cheng and Xue, 2021]	0.8135	0.4386	0.7730	0.3863	0.9616	0.2523	0.9801	0.1852
Ensemble	DCN [Wang et al., 2017]	0.8106	0.4414	0.7749	0.3855	0.9630	0.2162	0.9753	0.1676
	DeepFM [Guo et al., 2017]	0.8130	0.4389	0.7752	0.3859	0.9625	0.2520	0.9759	0.1993
	xDeepFM [Lian et al., 2018]	0.8127	0.4392	0.7747	0.3841	0.9612	0.2186	0.9779	0.1869
	DRIN [Jun et al., 2022]	0.8136	0.4385	0.7729	0.3860	0.9703	0.1998	0.9812	0.1592
	MaskNet [Wang et al., 2021b]	0.8137	0.4383	0.7731	0.3859	0.9706	0.1992	0.9819	0.1586
	DCN-V2 [Wang et al., 2021a]	0.8133	0.4393	0.7737	0.3840	0.9675	0.2131	0.9778	0.1910
	LightDIL [Zhang et al., 2023]	0.8138	0.4382	0.7751	0.3841	0.9711	0.1993	0.9834	0.1549
	FinalMLP [Mao et al., 2023]	0.8139	0.4380	0.7754	0.3837	0.9713	0.1989	0.9836	0.1546
	FINAL [Zhu et al., 2023]	0.8141	0.4379	0.7756	0.3831	0.9708	0.1996	0.9830	0.1567
GDCN [Wang et al., 2023]	0.8144	0.4374	0.7758	0.3829	0.9717	0.1984	0.9844	0.1538	
Ours	RE-SORT	0.8163**	0.4358**	0.7779**	0.3806**	0.9734**	0.1956**	0.9865**	0.1501**
	Rel. Imp	0.0019	-0.0016	0.0021	-0.0023	0.0017	-0.0028	0.0021	-0.0037

Table 2: Overall performance comparison in the four datasets. The t-test results show that our performance advantage over the previous SOTA method is statistically significant. The improvement is statistically significant with $p < 10^{-2}$ (\star); $p < 10^{-2}$, $\star\star$: $p < 10^{-4}$. “Rel. Imp” denotes the relative improvements compared with the previous SOTA method.

datasets. To mitigate overfitting, we implement early stopping based on the AUC attained on the validation dataset. In the D-SR and S-SR, we define the attenuation coefficient r as $[\frac{31}{32}, \frac{63}{64}, \dots, \frac{2^{M+5}-1}{2^{M+5}}]$.

4.2 COMPARISON WITH THE SOTA METHODS

We classify twenty competitive approaches into four categories: first-order, second-order, high-order, and ensemble methods. To ensure a fair comparison, we run each method 10 times with random seeds on a single GPU (NVIDIA A100) and report the average testing performance. Then, we conduct two-tailed t-tests [Liu et al., 2019] to compare the performance. As shown in Table 2, on all four datasets, RE-SORT outperforms all the other models in terms of both AUC and LogLoss, which validates its generalization ability. The greatest improvement is observed for the Avazu and Frappe, where RE-SORT exhibits a relative improvement of 0.21% over the second-best-performing GDCN. Previous two-stream methods such as FinalMLP and GDCN exhibit robust performance, while our RE-SORT constructs more effective multilevel features while eliminating spurious correlations and achieves the best performance. It is crucial to emphasize the significance of accurate CTR prediction, particularly in applications with substantial user bases; even a 0.1% AUC increase, although seemingly modest, can have a substantial impact, significantly boosting overall revenue [Cheng et al., 2016, Wang et al., 2017, Ling et al.,

2017]⁴. Moreover, compared to the previous SOTA model (GDCN), RE-SORT is almost 4 times faster, highlighting an additional valuable improvement, which is explained in detail in the following section.

Model	Avazu	MovieLens	UGC
GDCN	40	1.8	105
Baseline [4.1.1]	35	1.4	96
FinalMLP	30	1.1	87
Baseline + SA [4.1.1]	25	1.0	72
LightDIL	20	0.9	64
DRIN	16	0.8	50
RE-SORT	10	0.4	24

Table 3: Inference time (second) comparison on the test set.

Speed comparison. The rapid inference speed of the RE-SORT is attributed to its MSR structure. The SCE module does not affect the inference speed because it is used only during training. We choose “Baseline”; “Baseline + SA”; and the cutting-edge two-stream GDCN, FinalMLP, LightDIL, and DRIN methods for comparison. Table 3 demonstrates that our RE-SORT substantially outperforms the previous SOTA methods; it outperforms DRIN, the fastest among these methods, by approximately 90%.

⁴The GDCN yields a 0.17% improvement over the previous SOTA approach on Criteo. With its stacked structure, GDCN achieves a 0.04% improvement over the baseline.

Model	Criteo		Avazu		UGC	
	AUC \uparrow	Logloss \downarrow	AUC \uparrow	Logloss \downarrow	AUC \uparrow	Logloss \downarrow
Previous SOTA (GDCN)	0.8144	0.4374	0.7758	0.3829	0.8037	0.4055
Baseline [4.1.1]	0.8138	0.4387	0.7752	0.3845	0.8033	0.4064
Baseline + SA [4.1.1]	0.8140	0.4384	0.7753	0.3842	0.8035	0.4059
Baseline + MSR	0.8152	0.4377	0.7764	0.3827	0.8046	0.4044
Baseline + SCE	0.8154	0.4363	0.7770	0.3818	0.8053	0.4035
Full Approach (MSR + SCE)	0.8163**	0.4358**	0.7779**	0.3806**	0.8058**	0.4027**

Table 4: Ablation study of the RE-SORT. ‘‘Baseline + MSR’’ denotes that the two-stream MLP network of ‘‘Baseline’’ is replaced by MSR, and the implementation of these models can be found in our code. The last row is our full approach.

4.3 ABLATION STUDY

We verify the effectiveness of the MSR and the SCE structures through extensive experiments.

Improvement achieved with the MSR and SCE. Table 4 shows that MSR and SCE stably improve the performance of the model, exceeding the ‘‘Baseline’’ by an average of 0.25% in terms of the AUC across all three datasets. To fairly compare the performances of various two-stream structures, the results presented in the table are the best experimental results obtained with different depth combinations for the two streams within their corresponding network structures. Our MSR outperforms the two-stream MLP and two-stream SA structures by an average of 0.12% and 0.11% AUC, respectively. Tables 3 and 4 demonstrate that the proposed MSR structure outperforms MLP and attention-based models in terms of both accuracy and computational efficiency. An online A/B test is reported in the supplementary material, and we achieve an average enhancement of 1.62% over the baseline method.

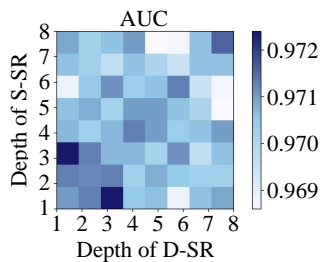
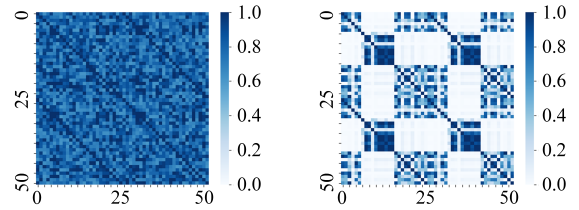


Figure 3: Performance with different MSR depths.

Two streams in MSR with different depths. We verify the performance of RE-SORT with different combinations of the S-SR and D-SR streams at various depths. On the five datasets, the best performance is obtained with D-SR and S-SR depths of 3 and 1, respectively. Figure 3 shows a visualization example based on the MovieLens dataset. When the D-SR and S-SR depths are the same (1, 2, and 3), the AUC performance is similar to that of the ‘‘Baseline’’ (0.9712, 0.9713, and 0.9711 vs. 0.9711), which shows that the MSR structure is not able to construct multilevel features with



(a) Feature correlation of ‘‘Baseline’’ on Avazu. (b) Feature correlation of SCE on Avazu.

Figure 4: Spurious correlation elimination of RE-SORT.

the same stacking depth to achieve improved performance. When the depths of the D-SR and S-SR streams are set to 3 and 1, respectively, the result is 0.12% greater than that of the ‘‘Baseline’’. Additional ablation experiments concerning the MSR are reported in the supplemental materials.

Feature visualization for SCE. We randomly select variables with 50 dimensions from input features of the CTR predictor learned by ‘‘Baseline’’ and SCE. Figure 4 shows that the correlations among the features are eliminated by SCE, while the model performance is notably improved. To a certain extent, this experiment substantiates that SCE can promote the model to identify critical features and acquire more effective associations with CTR predictions, thus enhancing the generalization ability. Additional experiments, such as a comparative analysis under out-of-distribution (OOD) settings, are reported in supplemental materials.

5 CONCLUSION

We introduce the RE-SORT for CTR prediction. The proposed MSR enables the network to efficiently capture diverse high-order representations. An SCE module is introduced to effectively remove spurious correlations, allowing the model to focus on true causal features. Extensive experiments on four public datasets, our production dataset, and the online A/B test demonstrate the SOTA performance of RE-SORT, which advances the current methods and offers valuable insights for future research and applications.

References

- Hyojin Bahng, Sanghyuk Chun, Sangdoon Yun, Jaegul Choo, and Seong Joon Oh. Learning de-biased representations with biased representations. In *ICML*, 2020.
- Mathieu Blondel, Akinori Fujino, Naonori Ueda, and Masakazu Ishihata. Higher-order factorization machines. *NeurIPS*, 2016.
- Heng-Tze Cheng, Levent Koc, Jeremiah Harmsen, Tal Shaked, Tushar Chandra, Hrishi Aradhye, Glen Anderson, Greg Corrado, Wei Chai, Mustafa Ispir, et al. Wide & deep learning for recommender systems. In *DLRS workshops*, 2016.
- Weiyu Cheng, Yanyan Shen, and Linpeng Huang. Adaptive factorization network: Learning adaptive-order feature interactions. In *AAAI*, 2020.
- Yuan Cheng and Yanbo Xue. Looking at ctr prediction again: Is attention all you need? In *SIGIR*, 2021.
- Shihan Dou, Rui Zheng, Ting Wu, Songyang Gao, Junjie Shan, Qi Zhang, Yueming Wu, and Xuanjing Huang. Decorrelate irrelevant, purify relevant: Overcome textual spurious correlations from a feature perspective. *arXiv preprint*, 2022.
- Hongzhi Du, Yanyan Li, Yanbiao Sun, Jigui Zhu, and Federico Tombari. Srh-net: Stacked recurrent hourglass network for stereo matching. *RA-L*, 2021.
- Ziwei Fan, Hao Ding, Anoop Deoras, and Trong Nghia Hoang. Personalized federated domain adaptation for item-to-item recommendation. In *UAI*, 2023.
- Kenji Fukumizu, Arthur Gretton, Xiaohai Sun, and Bernhard Schölkopf. Kernel measures of conditional dependence. *NeurIPS*, 2007.
- A Gretton, K Fukumizu, CH Teo, L Song, B Schölkopf, and A Smola. A kernel statistical test of independence, 2008.
- Fei Guan, Cheng Qian, and Feiyan He. A knowledge distillation-based deep interaction compressed network for ctr prediction. *Knowledge-Based Systems*, 2023.
- Huifeng Guo, Ruiming Tang, Yunming Ye, Zhenguo Li, and Xiuqiang He. Deepfm: a factorization-machine based neural network for ctr prediction. *arXiv preprint*, 2017.
- Xiangnan He and Tat-Seng Chua. Neural factorization machines for sparse predictive analytics. In *SIGIR*, 2017.
- Yue He, Xinwei Shen, Renzhe Xu, Tong Zhang, Yong Jiang, Wenchao Zou, and Peng Cui. Covariate-shift generalization via random sample weighting. In *AAAI*, 2023.
- Yuchin Juan, Yong Zhuang, Wei-Sheng Chin, and Chih-Jen Lin. Field-aware factorization machines for ctr prediction. In *RecSys*, 2016.
- Xie Jun, Zhao Xudong, Xu Xinying, Han Xiaoxia, Ren Jinchang, and Li Xingbing. Drin: Deep recurrent interaction network for click-through rate prediction. *Information Sciences*, 2022.
- Diederik P Kingma and Max Welling. Auto-encoding variational bayes. *arXiv preprint*, 2013.
- Yunqi Li, Hanxiong Chen, Juntao Tan, and Yongfeng Zhang. Causal factorization machine for robust recommendation. In *JCDL*, 2022.
- Jianxun Lian, Xiaohuan Zhou, Fuzheng Zhang, Zhongxia Chen, Xing Xie, and Guangzhong Sun. xdeepfm: Combining explicit and implicit feature interactions for recommender systems. In *SIGKDD*, 2018.
- Xiaoliang Ling, Weiwei Deng, Chen Gu, Hucheng Zhou, Cui Li, and Feng Sun. Model ensemble for click prediction in bing search ads. In *World Wide Web companion*, 2017.
- Bin Liu, Ruiming Tang, Yingzhi Chen, Jinkai Yu, Huifeng Guo, and Yuzhou Zhang. Feature generation by convolutional neural network for click-through rate prediction. In *WWW*, 2019.
- Chaochao Lu, Yuhuai Wu, José Miguel Hernández-Lobato, and Bernhard Schölkopf. Invariant causal representation learning for out-of-distribution generalization. In *ICLR*, 2021.
- Kelong Mao, Jieming Zhu, Liangcai Su, Guohao Cai, Yuru Li, and Zhenhua Dong. Finalmlp: An enhanced two-stream mlp model for ctr prediction. *arXiv preprint*, 2023.
- Junwei Pan, Jian Xu, Alfonso Lobos Ruiz, Wenliang Zhao, Shengjun Pan, Yu Sun, and Quan Lu. Field-weighted factorization machines for click-through rate prediction in display advertising. In *WWW*, 2018.
- Razvan Pascanu, Caglar Gulcehre, Kyunghyun Cho, and Yoshua Bengio. How to construct deep recurrent neural networks. *arXiv preprint*, 2013.
- Yanru Qu, Han Cai, Kan Ren, Weinan Zhang, Yong Yu, Ying Wen, and Jun Wang. Product-based neural networks for user response prediction. In *ICDM*, 2016.
- Massimo Quadrana, Alexandros Karatzoglou, Balázs Hidasi, and Paolo Cremonesi. Personalizing session-based recommendations with hierarchical recurrent neural networks. In *RecSys*, 2017.
- Prajit Ramachandran, Barret Zoph, and Quoc V Le. Swish: a self-gated activation function. *arXiv preprint*, 2017.

- Steffen Rendle. Factorization machines. In *ICDM*, 2010.
- Steffen Rendle, Christoph Freudenthaler, Zeno Gantner, and Lars Schmidt-Thieme. Bpr: Bayesian personalized ranking from implicit feedback. In *UAI*, 2009.
- Matthew Richardson, Ewa Dominowska, and Robert Ragno. Predicting clicks: estimating the click-through rate for new ads. In *WWW*, 2007.
- Mohammad Shoeybi, Mostofa Patwary, Raul Puri, Patrick LeGresley, Jared Casper, and Bryan Catanzaro. Megatron-LM: Training multi-billion parameter language models using model parallelism. *arXiv preprint*, 2019.
- Weiping Song, Chence Shi, Zhiping Xiao, Zhijian Duan, Yewen Xu, Ming Zhang, and Jian Tang. AutoInt: Automatic feature interaction learning via self-attentive neural networks. In *CIKM*, 2019.
- Peter L Spirtes, Christopher Meek, and Thomas S Richardson. Causal inference in the presence of latent variables and selection bias. *arXiv preprint*, 2013.
- Eric V Strobl, Kun Zhang, and Shyam Visweswaran. Approximate kernel-based conditional independence tests for fast non-parametric causal discovery. *Journal of Causal Inference*, 2019.
- Yang Sun, Junwei Pan, Alex Zhang, and Aaron Flores. Fm2: Field-matrixed factorization machines for recommender systems. In *WWW*, 2021.
- Yutao Sun, Li Dong, Barun Patra, Shuming Ma, Shaohan Huang, Alon Benhaim, Vishrav Chaudhary, Xia Song, and Furu Wei. A length-extrapolatable transformer. *arXiv preprint*, 2022.
- Fangye Wang, Hansu Gu, Dongsheng Li, Tun Lu, Peng Zhang, and Ning Gu. Towards deeper, lighter and interpretable cross network for ctr prediction. In *CIKM*, 2023.
- Ruoxi Wang, Bin Fu, Gang Fu, and Mingliang Wang. Deep & cross network for ad click predictions. In *ADKDD*, 2017.
- Ruoxi Wang, Rakesh Shivanna, Derek Cheng, Sagar Jain, Dong Lin, Lichan Hong, and Ed Chi. Dcn v2: Improved deep & cross network and practical lessons for web-scale learning to rank systems. In *WWW*, 2021a.
- Zhiqiang Wang, Qingyun She, and Junlin Zhang. Masknet: Introducing feature-wise multiplication to ctr ranking models by instance-guided mask. *arXiv preprint*, 2021b.
- Jun Xiao, Hao Ye, Xiangnan He, Hanwang Zhang, Fei Wu, and Tat-Seng Chua. Attentional factorization machines: Learning the weight of feature interactions via attention networks. *arXiv preprint*, 2017.
- En Xu, Zhiwen Yu, Bin Guo, and Helei Cui. Core interest network for click-through rate prediction. *TKDD*, 2021a.
- Renzhe Xu, Peng Cui, Zheyang Shen, Xingxuan Zhang, and Tong Zhang. Why stable learning works? a theory of covariate shift generalization. *arXiv preprint*, 2021b.
- Renzhe Xu, Xingxuan Zhang, Zheyang Shen, Tong Zhang, and Peng Cui. A theoretical analysis on independence-driven importance weighting for covariate-shift generalization. In *ICML*, 2022.
- Mao Ye, Ruichen Jiang, Haoxiang Wang, Dhruv Choudhary, Xiaocong Du, Bhargav Bhushanam, Aryan Mokhtari, Arun Kejariwal, and Qiang Liu. Future gradient descent for adapting the temporal shifting data distribution in online recommendation systems. In *UAI*, 2022.
- Xingxuan Zhang, Peng Cui, Renzhe Xu, Linjun Zhou, Yue He, and Zheyang Shen. Deep stable learning for out-of-distribution generalization. In *CVPR*, 2021.
- Yang Zhang, Tianhao Shi, Fuli Feng, Wenjie Wang, Dingxian Wang, Xiangnan He, and Yongdong Zhang. Reformulating ctr prediction: Learning invariant feature interactions for recommendation. *arXiv preprint*, 2023.
- Xiao Zhou, Yong Lin, Renjie Pi, Weizhong Zhang, Renzhe Xu, Peng Cui, and Tong Zhang. Model agnostic sample reweighting for out-of-distribution learning. In *ICML*, 2022.
- Jieming Zhu, Jinyang Liu, Shuai Yang, Qi Zhang, and Xiquang He. Open benchmarking for click-through rate prediction. In *CIKM*, 2021.
- Jieming Zhu, Qinglin Jia, Guohao Cai, Quanyu Dai, Jingjie Li, Zhenhua Dong, Ruiming Tang, and Rui Zhang. Final: Factorized interaction layer for ctr prediction. In *SIGIR*, 2023.

RE-SORT: Removing Spurious Correlation in Multilevel Interaction for CTR Prediction

(Supplementary Material)

A ADDITIONAL EXPERIMENT RESULTS

Online evaluation. We implement the RE-SORT framework across various commercial scenarios within our enterprise, driven by its significant performance improvements and minimal latency overhead. In our commercial gaming content recommendation environment, catering to the engagement of millions of daily active users exploring diverse gaming materials, we conducted a comprehensive A/B test over a week, starting from November 15th to November 21st, 2023. For the online deployment phase, we allocated 5% of the total traffic to the experimental group, encompassing more than 500,000 active users. A meticulous comparative analysis was performed between our proposed method and the carefully designed: “Baseline” model. The online outcomes obtained over the 7-day period are concisely depicted in Table 5. Remarkably, our model consistently improved different online engagement metrics during the evaluation period, with an average improvement of 1.62%. The online inference latency experienced a manageable increase of 68.96%. These experimental results provide substantial evidence for the effectiveness of the RE-SORT framework.

	Day1	Day2	Day3	Day4	Day5	Day6	Day7	Average
Δ CTR	1.43%	1.56%	1.79%	1.82%	1.78%	1.58%	1.37%	1.62%

Table 5: Results of a seven-day online A/B test.

Analysis of the performance variance. We analyze the performance variance of our model in comparison to that of three representative SOTA models: FinalMLP [Mao et al., 2023], FINAL [Zhu et al., 2023] and GDCN [Wang et al., 2023]. We carried out 10 experiments for each model on each dataset. As depicted in Figure 5, our model consistently outperforms and exhibits the greatest stability across different datasets compared to the other methods.

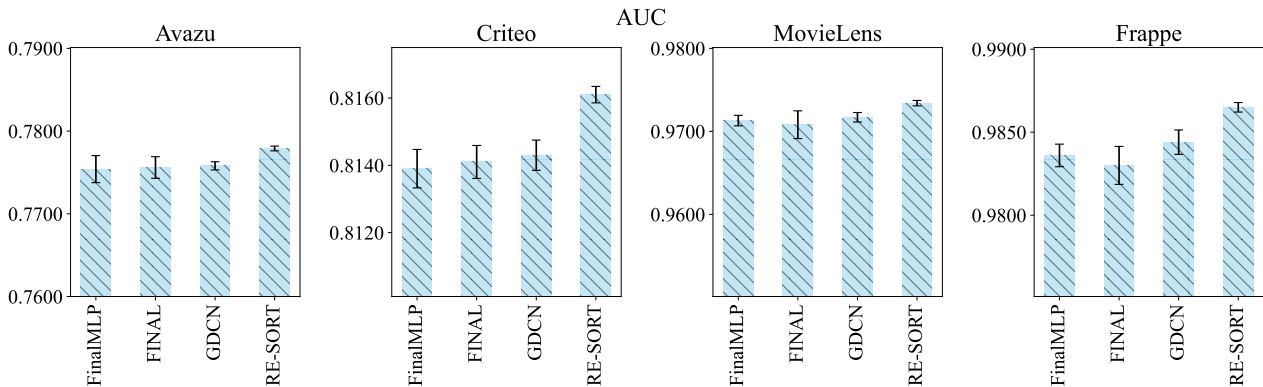


Figure 5: Variance comparison of different SOTA models.

Performance comparison among the proposed recurrent (RE) block, MLP block, and self-attention (SA) block. To provide additional evidence that the proposed recurrent (RE) block within the MSR structure can more effectively extract distinct features than traditional MLP and SA blocks, we carry out an experiment that involves stacking of different types of blocks in single-stream networks and evaluating their performance (AUC) on the Criteo dataset and our UGC dataset. As illustrated in Table 6, our recurrent block consistently outperforms the other two methods across various stacking configurations, which indicates that replacing the MLP and SA structures with the proposed recurrent structure can facilitate the extraction of more effective features, resulting in enhanced performance.

Model	Block number = 1		Block number = 2		Block number = 3		Block number = 4	
	Criteo	UGC	Criteo	UGC	Criteo	UGC	Criteo	UGC
MLP block	0.8110	0.8004	0.8117	0.8014	0.8115	0.8012	0.8112	0.8007
SA block	0.8115	0.8011	0.8125	0.8019	0.8123	0.8017	0.8119	0.8015
RE block	0.8128**	0.8018**	0.8133**	0.8021**	0.8136**	0.8028**	0.8132**	0.8024**

Table 6: Performance (AUC) comparison among our proposed stacked recurrent (RE) block, the stacked MLP block, and the stacked self-attention (SA) block within a single stream. The implementations of different types of blocks can be found in our open-source code.

Different numbers of random Fourier spaces (RFSs). We analyze the influence of using different numbers of RFSs. In Figure 6, the light blue columns show the different AUCs obtained using different numbers of fixed RFSs (1~8) on MovieLens and Avazu. Through extensive experiments, we further find that compared to utilizing a fixed number of RFSs, using decreasing numbers of RFSs in each epoch further yields improved performance. The dark blue columns show the performance achieved with decreasing numbers of RFSs, and the horizontal axis represents the maximum value (the number of RFSs uniformly decreases from the maximum value to 1 in each epoch).

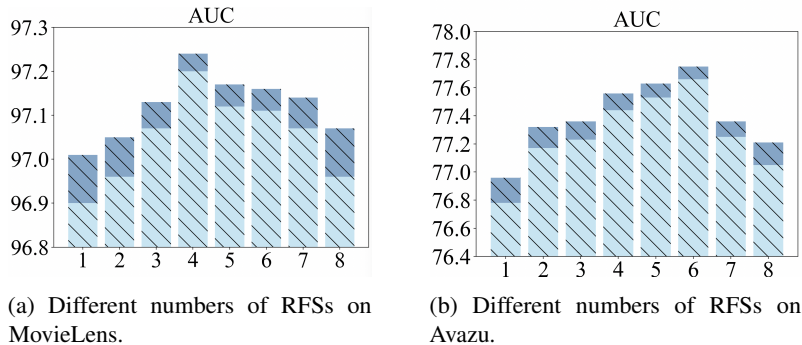


Figure 6: Comparison of using fixed number (light blue) and decreasing numbers (dark blue) of RFS.

Comparison experiment involving the SCE module and its variants. Although utilizing the Laplacian kernel method and sample weighting to handle the disturbance terms contained in the input data is a promising approach, several straightforward alternatives, such as regularization and variational auto-encoder (VAE) [Kingma and Welling, 2013], are available. We also conduct comparative experiments. As shown in Table 7, our SCE module outperforms the other methods by a large margin, which validates its effectiveness in handling the disturbance terms for accurate CTR prediction.

Comparison experiment involving the MSR structure and its variants. To further demonstrate the effectiveness of the two-stream MSR structure, we construct single-stream and three-stream variants based on the proposed stacked recurrent structure (“Single-stream SR” and “Three-stream SR”) for comparative experiments. Over multiple experiments, we report the best performances attained by the single-stream and three-stream variants under different stacking depths in Table 8. We also compare the performance of two-stream and single-stream networks under the same multilevel conditions. Specifically, we add an expanded single-stream (“Ex. Single-stream SR”) model that uses a skip layer to merge features from different layers for prediction. The best result is achieved by merging features from the first and third (last) layers. Table 8 shows that our proposed two-stream MSR structure outperforms the other variants in terms of accuracy, and the two-stream network also has fewer model parameters (“Param.”) than does the three-stream network. This experiment demonstrates that blindly

Model	Criteo		Avazu		UGC	
	AUC \uparrow	Logloss \downarrow	AUC \uparrow	Logloss \downarrow	AUC \uparrow	Logloss \downarrow
Baseline [4.1.1]	0.8138	0.4387	0.7752	0.3845	0.8033	0.4064
Baseline + Regularization	0.8134	0.4395	0.7746	0.3854	0.8030	0.4068
Baseline + VAE	0.8140	0.4381	0.7755	0.3840	0.8035	0.4060
Baseline + SCE	0.8154**	0.4363**	0.7770**	0.3818**	0.8053**	0.4035**

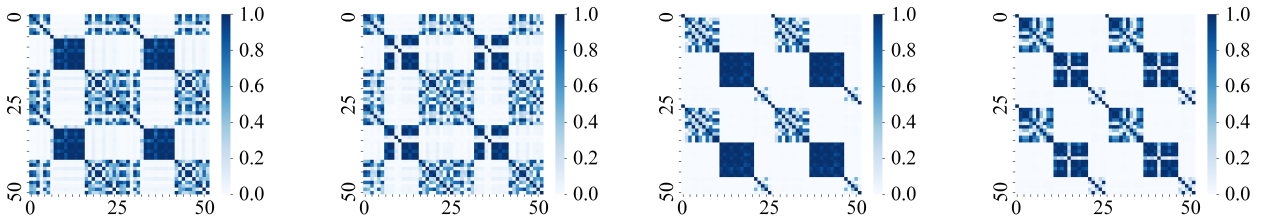
Table 7: Ablation study of the proposed SCE module based on the Criteo, Avazu, and UGC datasets.

increasing the depth and width does not enhance the performance of the network; instead, it leads to an increase in the number of model parameters.

Model	Criteo			Avazu			UGC		
	AUC \uparrow	Logloss \downarrow	Param.	AUC \uparrow	Logloss \downarrow	Param.	AUC \uparrow	Logloss \downarrow	Param.
Baseline [4.1.1]	0.8138	0.4387	23.6M	0.7752	0.3845	14.7M	0.8033	0.4064	29.0M
Single-stream SR	0.8136	0.4392	9.3M	0.7749	0.3851	5.0M	0.8028	0.4068	10.9M
Ex. Single-stream SR	0.8138	0.4389	10.4M	0.7753	0.3846	7.1M	0.8031	0.4067	13.3M
Three-stream SR	0.8148	0.4372	28.4M	0.7760	0.3836	16.1M	0.8043	0.4049	34.5M
Two-stream (MSR)	0.8152**	0.4377**	19.0M	0.7764**	0.3827**	11.2M	0.8046**	0.4044**	24.1M

Table 8: Ablation study of different number of streams based on the Criteo, Avazu, and UGC datasets.

Feature correlation visualizations of the S-SR and D-SR streams. We randomly chose 50 feature variables from both the Avazu and Frappe datasets. The feature correlation maps of the S-SR and D-SR streams are depicted in Figure 7. As illustrated in the figure, noticeable difference exist between the two feature correlation maps across both datasets.



(a) Feature correlation of S-SR on the Avazu dataset. (b) Feature correlation of D-SR on the Avazu dataset. (c) Feature correlation of S-SR on the Frappe dataset. (d) Feature correlation of D-SR on the Frappe dataset.

Figure 7: Feature visualization of D-SR and S-SR.

B COMPARATIVE ANALYSIS UNDER OUT-OF-DISTRIBUTION (OOD) SETTINGS

Dataset settings. Another contributing factor to the issue of spurious correlation is the distributional discrepancy between the training and test sets. To further validate the effectiveness of the SCE module, we simulate a larger distribution shift between the training set and the test set. We create OOD testing sets using UGC data. We generate different data distributions by altering the bias rate ρ , where $\rho > 1$ implies a positive correlation between the click behavior and noisy features, and $\rho < -1$ implies a negative correlation. The higher $|\rho|$ is, the stronger the correlation between the click behavior and noisy features. Therefore, different values of ρ refer to different environments.

For instance, if the training set is more likely to collect data from young male users, features like low payment and a history of clicking on sports game content may exhibit spurious correlation due to their increased likelihood of co-occurrence. These are important features for predicting whether sports game content will be clicked. However, the test set covers users of all

ages and genders, and the correlation between low payment and a history of clicking on sports game content ceases to exist. As a result, within the test set, low payment becomes an erroneous feature, leading to a decrease in generalization ability.

To evaluate the generalization ability of our RE-SORT model, we use the data generated with $\rho = 2.5$ as the default training data, and the test data obtained with $\rho = 2.5^\dagger$ can be regarded as the independent identical distributed (IID) data. We use the data with different values of $\rho \in \{-3.0, -2.5, -1.5, 1.5, 2.5, 3.0\}$ as test data from different environments. To benchmark our approach against other causality-based recommendation methods, we implement the CFM method [Li et al., 2022] in the context of the CTR task and incorporate it into our comparative analysis.

Evaluation. In Table 9, we observe that all methods show performance drops when moving from the IID testing setting to the OOD testing setting. This is a common occurrence due to the significant distribution shifts between the training set and the OOD testing set. As the distribution discrepancy between the testing set and the training set increases, the AUC of all methods gets worse. However, our methods demonstrate success in mitigating this performance degradation and outperform other causality-based approaches (LightDIL [Zhang et al., 2023] and CFM [Li et al., 2022]). The final row of the table highlights the improvement of RE-SORT compared to LightDIL.

Model	$\rho = -3$	$\rho = -2.5$	$\rho = -1.5$	$\rho = 1.5$	$\rho = 2.5^\dagger$	$\rho = 3$
Baseline	0.7008	0.7326	0.7491	0.7831	0.8033	0.7818
GDCN	0.7082	0.7436	0.7541	0.7873	0.8037	0.7865
CFM	0.7117	0.7498	0.7623	0.7855	0.8032	0.7849
LightDIL	0.7248	0.7542	0.7641	0.7860	0.8035	0.7866
Baseline + SCE	0.7403	0.7637	0.7691	0.7903	0.8053	0.7882
RE-SORT	0.7450 **	0.7694 **	0.7759 **	0.7943 **	0.8058 **	0.7931 **
Rel. Imp	0.0202	0.0152	0.0118	0.0083	0.0023	0.0065

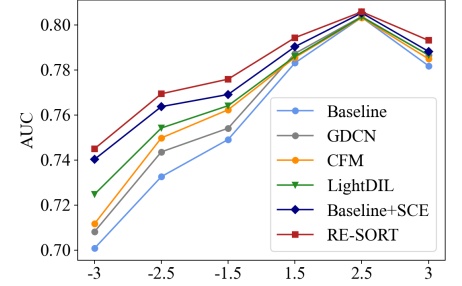


Table 9: Performance of different models under the OOD settings.

C ADDITIONAL DEFINITIONS, ASSUMPTIONS, AND THEOREMS FOR THE SCE MODULE

C.1 SAMPLE REWEIGHTING

Assumption 1 indicates that the correlation between FM_{rob} and $g(FM_{\text{rob}})$ has lower variation than that between FM_{fal} and $g(FM_{\text{rob}})$ when subjected to parameter variance.

Assumption 1. For all P' uniformly sampled from \mathcal{P} , the following condition holds: $Var[\mathbb{E}_{P'}(FM_{\text{rob}}g(FM_{\text{rob}}))] < Var[\mathbb{E}_{P'}(FM_{\text{fal}}g(FM_{\text{rob}}))]$.

Theorem 1 He et al. [2023] demonstrates that when we apply sample weighting even in a random way, the estimation of $\beta_{FM_{\text{rob}}}$ is more robust and exhibits less variation in comparison to $\beta_{FM_{\text{fal}}}$.

Theorem 1. Let $\beta_{FM_{\text{rob}}}^{\sim}$ and $\beta_{FM_{\text{fal}}}^{\sim}$ be the components of $\tilde{\beta}$ corresponding to FM_{rob} and FM_{fal} respectively. Under Assumption 3.5.1, we have $Var(\beta_{FM_{\text{rob}}}^{\sim}) < Var(\beta_{FM_{\text{fal}}}^{\sim})$.

We define the minimal robust features set.

Definition 1. minimal robust features set: A minimal robust features set of predicting Y under training distribution P^{train} is any subset FM_{rob} of FM satisfying the following equation, and no proper subsets of FM_{rob} satisfies it:

$$\mathbb{E}_{P^{\text{train}}}[Y|FM_{\text{rob}}] = \mathbb{E}_{P^{\text{train}}}[Y|FM]. \quad (19)$$

It can also be formulated as:

$$Y \perp FM_{\text{fal}} | FM_{\text{rob}},$$

where $Y \perp FM_{\text{fal}}$ means Y and FM_{fal} are statistically independent of each other.

It has been proven that FM_{rob} is the minimal and optimal predictor if and only if FM_{rob} is the minimal robust feature [Xu et al., 2022]. Therefore, we intend to capture the minimal robust feature set FM_{rob} for robust prediction. We denote the robust feature set as the minimal robust feature set for simplicity.

Definition 2. *Sample weighting function: Let \mathcal{W} be the set of sample weighting functions that satisfy:*

$$\mathcal{W} = \{w : \text{FM} \rightarrow \mathbb{R}^+ | E_{P^{\text{train}}(\text{FM})}[w(\text{FM})] = 1\}. \quad (20)$$

Then $\forall w \in \mathcal{W}$, the corresponding weighted distribution is $\tilde{P}_w(\text{FM}, Y) = w(\text{FM})P^{\text{train}}(\text{FM}, Y)$, \tilde{P}_w is well defined with the same support of P^{train} . What we want is actually \mathcal{W}_\perp : the subset of \mathcal{W} in which FM are mutually independent.

Lemma 1. *Existence of a “debiased” weighting function [Zhou et al., 2022]. Consider $\text{FM}=[\text{FM}_{\text{rob}}, \text{FM}_{\text{fal}}]$. We want to fit a linear model $\theta^T \text{FM}$ to predict y . Given infinite data in the training dataset D_{train} , there exists a weight function $w \in \mathcal{W}$, i.e.,*

$$w(\text{FM}, y) = \frac{\mathbb{P}(\text{FM}_{\text{rob}}, y)\mathbb{P}(\text{FM}_{\text{fal}})}{\mathbb{P}(\text{FM}_{\text{rob}}, \text{FM}_{\text{fal}}, y)}, \quad (21)$$

such that the solution satisfies that

$$\theta^*(w) = \bar{\theta} = [\bar{\theta}_{\text{FM}_{\text{rob}}}; 0], \quad (22)$$

where $\bar{\theta}_{\text{FM}_{\text{rob}}}$ is the optimal model that merely uses FM_{rob} , i.e.,

$$\bar{\theta}_{\text{FM}_{\text{rob}}} := \arg \min_{\theta \in \mathbb{R}^{d_{\text{FM}_{\text{rob}}}}} \mathbb{E}[(y - \theta^T \text{FM}_{\text{rob}})^2]. \quad (23)$$

Theorem 2. *No matter data generation is linear or nonlinear, robust features can be almost perfectly selected if conducting weighted least squares (WLS) using the weighting function in \mathcal{W}_\perp [Xu et al., 2021b].*

C.2 SCE

Here, we use X and Y denote random variables, the corresponding RKHS is denoted by \mathcal{H}_X and \mathcal{H}_Y . We define the cross-covariance operator \sum_{XY} from \mathcal{H}_Y to \mathcal{H}_X :

$$\begin{aligned} & \langle h_X, \sum_{XY} h_Y \rangle \\ &= \mathbb{E}_{XY}[h_X(X)h_Y(Y)] - \mathbb{E}_X[h_X(X)]\mathbb{E}_Y[h_Y(Y)] \end{aligned} \quad (24)$$

for all $h_X \in \mathcal{H}_X$ and $h_Y \in \mathcal{H}_Y$. Then, the independence can be determined by the following proposition [Fukumizu et al., 2007]:

Proposition 1. *If the product $k_X k_Y$ is characteristic, $\mathbb{E}[k_X(X, X)] < \infty$ and $\mathbb{E}[k_Y(Y, Y)] < \infty$, we have that $\mathbb{E}_{XY} = 0$ if and only if $X \perp Y$.*

The Hilbert-Schmidt independence criterion (HSIC) [Gretton et al., 2008], which necessitates that the squared Hilbert-Schmidt norm of \sum_{XY} be equal to zero, can be utilized as a criterion for supervising the elimination of spurious correlations [Bahng et al., 2020].

D RELATED METHODS

We classify the related CTR prediction methods into four types:

1. **First-Order:** LR [Richardson et al., 2007]. It models both first-order and second-order feature interactions.
2. **Second-Order:** FM [Rendle, 2010], AFM [Xiao et al., 2017]. They model both first-order and second-order interactions.
3. **High-Order:** HOFM [Blondel et al., 2016], NFM [He and Chua, 2017], OPNN [Qu et al., 2016], CIN [Xu et al., 2021a], AutoInt [Song et al., 2019], AFN [Cheng et al., 2020], SAM [Cheng and Xue, 2021]. They can model interactions higher than second-order.
4. **Ensemble:** DCN [Wang et al., 2017], DeepFM [Guo et al., 2017], xDeepFM [Lian et al., 2018], DRIN [Jun et al., 2022], MaskNet [Wang et al., 2021b], DCN-V2 [Wang et al., 2021a], LightDIL [Zhang et al., 2023], FINAL [Zhu et al., 2023], FinalMLP [Mao et al., 2023], GDCN [Wang et al., 2023]. These models adopt parallel or stacked structures to integrate different feature interaction methods.